Journal of Structural Geology, Vol. 13, No. 4, pp. 369 to 384, 1991
Printed in Great Britain

0191-8141/91 $03.00+0.00

Calcite textures: examples from nappes with strain-path partitioning

L. RATSCHBACHER,* H.-R. WENK and M. SINTUBIN†

Department of Geology and Geophysics, University of California, Berkeley, CA 94720, U.S.A.

(*Received* 15 *May* 1990; *accepted in revised form* 17 *October* 1990)

Abstract—Strain-path partitioning (partitioning of deformation into components of pure and simple shear) in two Alpine nappes is qualitatively indicated by a variation in orientation of foliation, microkinematic criteria, quartz textures, and a comparison with strain-path partitioning in theoretical nappe models. The degree of non-coaxial deformation relative to the total deformation is quantified by using the asymmetry of textures in calcite tectonites. The texture interpretation is based on both polycrystal plasticity models and experimental data.

Calcite tectonites in the Graz-Paleozoic thrust sheet (Austria) and the Morcles nappe (Switzerland) were deformed in a strain path with both pure and simple shear components. Texture asymmetry supports the strain path derived from geological observations. As an exception, a high-strain ultramylonite deformed nearly exclusively in pure shear. It is suggested that this represents a softening instability since deformation in pure shear is energetically more favorable than in simple shear. The incompatibilities caused by heterogeneous pure shear are accommodated by detachments and heterogeneous simple shear adjacent to the pure shear zone.

INTRODUCTION

IN THIS paper, we describe calcite textures from two nappes in the Alps for which the strain path (e.g. Hobbs *et al.* 1976) is geologically reasonably well defined. We first review the strain path, particularly the vertical partitioning into components of pure and simple shear ('strain-path partitioning'), in spreading–gliding nappes. In pure shear, principal axes of strain maintain their orientations relative to material points throughout the deformation; in simple shear, successive principal axes are not parallel, but rotate with respect to the material. We then show that the theoretical pattern closely fits the qualitatively established strain-path partitioning in the Graz-Paleozoic thrust sheet in the Austrian Alps. Next we compare the specific partitioning in spreading–gliding nappes with the vertical variation of calcite textures in sections across the base of the Graz-Paleozoic. The interpretation of calcite textures relies on a comparison of natural textures with those predicted from polycrystal plasticity models (e.g. Takeshita *et al.* 1987, Wenk *et al.* 1987, Tomé *et al.* in press) and obtained in experimental studies (e.g. Schmid *et al.* 1987, Wenk *et al.* 1987). The polycrystal plasticity theory enables us to use the calcite textures as sensitive indicators of strain path and to evaluate mechanical properties of the deformed polycrystals. In particular, texture variation in the Graz-Paleozoic thrust sheet emphasizes the heterogeneous nature of deformation and the importance of pure shear in narrow zones of concentrated deformation. We also compare the strain path and the calcite-texture data of the Graz-Paleozoic with those of the Morcles nappe in the Helvetic Alps (Switzerland) where both strain-path partitioning and textures of calcite tectonites have previously been investigated (e.g. Schmid *et al.* 1981, Dietrich & Song, 1984, Dietrich & Casey 1989).

GRAZ-PALEOZOIC THRUST SHEET (AUSTRIAN ALPS)

Theoretical setting: spreading–gliding nappes

In superficial nappes, viscous *spreading* describes flow of rocks under their own weight along a negligible basal slope and with a coherent contact allowing no slip along the sole (e.g. Elliott, 1976, Merle 1986, 1989, and references therein) (Fig. 1a insert). Viscous *gliding* characterizes gravity-induced nappe movement, again with a coherent basal contact, but along a basal slope inclined in the flow direction (e.g. Kehle 1970, Merle 1986, 1989, and references therein) (Fig. 1a insert). In spreading–gliding nappes the gliding process is superposed on the spreading one. A rigid sliding component (rigid body translation) along the sole thrust has no effect on the strain in the interior of the nappe. Internal strain and strain path can be described as follows (e.g. Merle 1986, 1989) (Fig. 1a): (1) vertical strain gradients are high and strain increases from top to bottom; (2) strain is accumulated by a combination of pure shear with the stretch parallel to the thrust plane and simple shear with the shearing plane also parallel to the thrust plane; (3) viscous gliding produces the simple shear component which increases (from the shear stress free surface of the nappe) downward toward the basal shear plane. Thinning of the nappe under its own weight during spreading is manifested by the pure shear component.

The strain-path partitioning into components of pure

*Permanent address: Institut für Geologie, Universität, D-7400 Tübingen, Germany.
†Permanent address: Instituut voor Aardwetenschappen, Katholieke Universiteit, 3000 Leuven, Belgium.

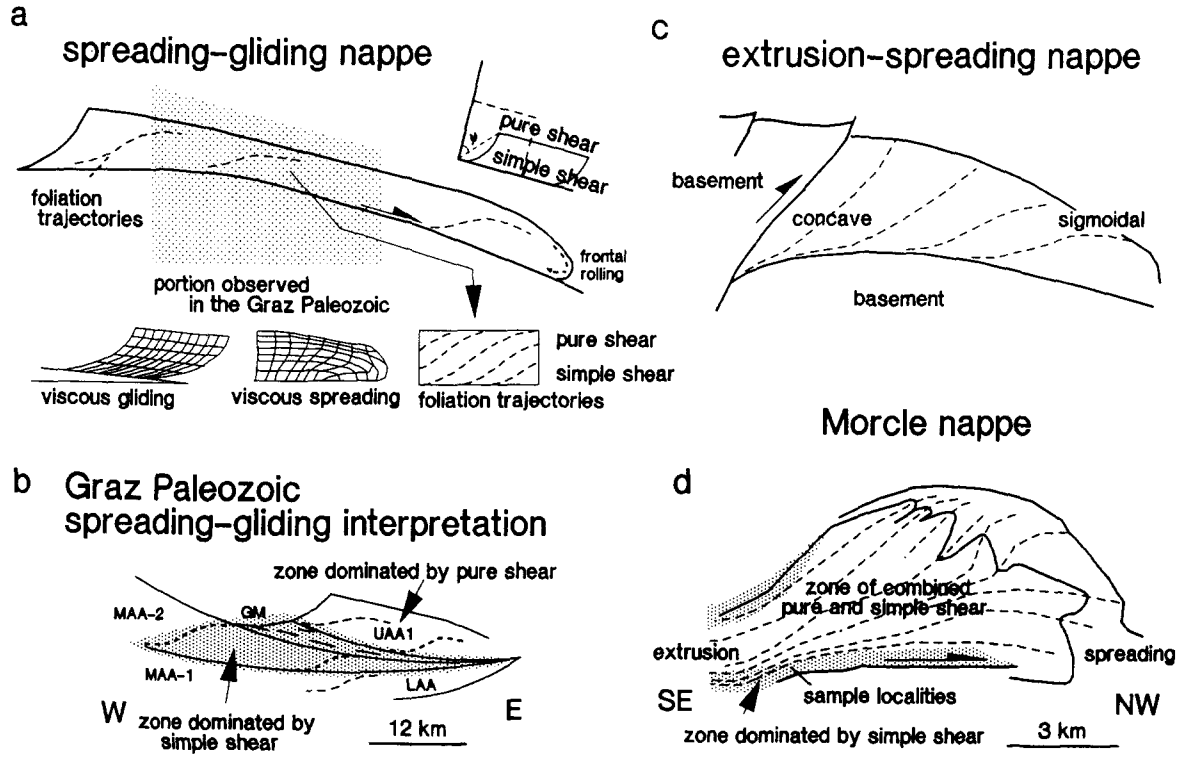

Fig. 1. (a) Principal features of spreading–gliding nappes modified from Merle (1986, 1989). Inserts show: internal strain as a combination of pure and simple shear (above right); strain pattern (visualized by deformation of an orthogonal grid) produced by viscous gliding (row, left side) and viscous spreading (row, center); typical stretch (foliation) trajectories in the central portion of the nappe (row, right). (b) Spreading–gliding nappe interpretation of section through Graz-Paleozoic (units GM and UAA1). (c) Extrusion–spreading model modified from Merle (1989). (d) Schematic section through the Morcles fold nappe showing strain trajectories (after Ramsay & Huber 1987). Shading in (b) and (d) indicates zones dominated by simple shear. UAA, MAA, LAA are Austroalpine basement units.

and simple shear within spreading–gliding nappes may be recognized in the field in vertical cross-sections parallel to transport direction. The orientation of the principal stretch is dependant on the value of the simple shear component. Sigmoidally curved stretch trajectories (foliation trajectories in three dimensions), with subhorizontal attitude at the top and bottom of the nappe and dipping attitude midway in the nappe (Fig. 1a), reflect a pure shear superposed by a heterogeneous simple shear (Ramsay & Graham 1970) with increasing strain intensity toward the bottom. This is in contrast to nappes produced by a horizontal push from the rear (e.g. Chapple 1978), in which stretch trajectories are subvertical (besides a basal high strain zone).

Natural setting: Graz-Paleozoic thrust sheet

Structural setting. The Graz-Paleozoic is part of the Upper Austroalpine unit, the uppermost thrust system of the Alpine orogenic belt. It was stacked in a westerly direction during the Early Cretaceous (±125 Ma, Fritz 1988). Structural overprinting demonstrates a reactivation by E-directed deformation which interferes with regional cooling of the Austroalpine units (Late Cretaceous, 80–60 Ma). This Late Cretaceous crustal thinning deformation in the eastern Eastern Alps was explained by unroofing caused by a gravitational instability of the Eastern Alpine orogenic wedge (see Platt 1986) after a major collisional phase (Ratschbacher *et al.* 1989). Dominantly coaxial stretching occurred in the basement units of deep tectonic position and in regions with medium-grade Alpine metamorphism. Klippen of Mesozoic cover rocks and low- to very low-grade basement units (e.g. the Graz-Paleozoic) show E-directed normal faults, and thrusts were reactivated as normal faults or shear zones with a normal fault geometry (Ratschbacher & Neubauer 1989). The formation of basins (the Gosau basins) indicates extension at highest structural levels.

Late Cretaceous deformation of the Graz-Paleozoic is concentrated at its base and a significant portion of mylonites encompass calcite tectonites. These calcite mylonites and ultramylonites ('*Grenzmarmor*' of the German literature) indicate a rheologically weak horizon along the sole thrust. We now compare the theoretical pattern of strain-path partitioning in spreading–gliding nappes with that of the Graz-Paleozoic. In the following structural description, we refer only to the Late Cretaceous deformation and its accompanying very low- to low-grade metamorphism. Mapping of structures, particularly of foliation, was difficult in several outcrops due to the presence of the pre-existing Early Cretaceous foliation.

In map view (Fig. 2), the Graz-Paleozoic is underlain along the western edge by a belt of mylonites up to a few hundred meters thick which reappears along its eastern edge as a zone up to a few tens of meters thick. Both belts are connected along the northern rim by a zone with strike-slip displacement; the southern rim is covered by Tertiary sediments. The three-dimensional

geometry of the mylonite belt is spoon-shaped. Results of field mapping and kinematic data are best discussed in three sections across the base of the Graz-Paleozoic (Figs. 3 and 4).

(1) At the western edge (Fig. 4, 1) mylonites encompass from bottom to top weakly deformed basement (MAA-1), mylonitized basement bound by detachments with normal fault geometry (MAA-2), a thin (≤20 m in the profile of section 1) layer of calcite-mylonites (Grenzmarmor, GM), and the main body of the Graz-Paleozoic bound basally by a detachment. In the latter, deformation intensity decreases rapidly upward (UAA-1). At the top of this wedge, the basin of the 'Gosau of Kainach' (Fig. 2) indicates subhorizontal extension at high crustal level. The basin fill was affected by extension as well. Figure 5(a) shows plots of fault–slickenside pairs at three sites and corresponding stress orientations calculated according to the direct inversion method of Angelier (1979) ('stress': following the entrenched terminology to call analysis of finite displacements along faults 'stress' or 'paleostress' analysis). The most compressive stress is subvertical.

(2) In a section in the southeast of the Graz-Paleozoic (Fig. 4-2), mylonitization is restricted to a zone of brittle–ductile deformation at the top of a basement unit (MAA-1) which is separated by a detachment from thin (≤10 m) calcite ultramylonites at the top (GM). The calcite ultramylonites rapidly grade into decreasingly deformed marbles of the main body of the Graz-Paleozoic (UAA-1). Non-penetrative brittle–ductile shear zones with normal fault geometry and predominantly westward shear indicate localized backflow above the main zone of eastward flow.

(3) A section in the northeast of the Graz-Paleozoic (Fig. 4, 3) consists of basement (LAA) in which deformation decreases rapidly downwards, a mylonitized basement sheet (0–100 m; MAA-2) bound by detachments in the middle, and upwards decreasingly deformed rocks of the main body of the Graz-Paleozoic at the top (UAA-1). Fault–slickenside pairs indicate subhorizontal extension of the uppermost unit (Fig. 5b).

In all three sections, foliations curve sigmoidally across high strain zones (Fig. 4 top row) imitating the sigmoidal shape of stretch trajectories in zones of heterogeneous simple shear (Ramsay & Graham 1970). Accordingly, we interpret the increase in strain toward the high strain zone along the base of the Graz-Paleozoic as accumulated by heterogeneous simple shear. Stretch trajectories attain subhorizontal attitude both in the main body of the Graz-Paleozoic and in the basement rocks of its footwall. This is indicated by subhorizontal orientation of both the least compressive stress (obtained from fault-slip analysis in the main body of the Graz-Paleozoic, Fig. 5) and the foliation. We interpret the horizontal attitude of the foliation in these weakly deformed areas, off the high strain zone at the base of the nappe, as a result of pure shear deformation.

Strain-path partitioning in components of pure and simple shear along the base of the Graz-Paleozoic was further explored by small-scale kinematic criteria (e.g. Fig. 3, bottom right) and quartz microfabrics (Fig. 4, lower part). Monoclinic quartz textures, typical for a strain path dominated by simple shear, occur within the basal mylonites of the Graz-Paleozoic, and orthorhombic textures, indicative of pure shear strain-paths, dominate in the hanging wall and the footwall (Fig. 4, lower part). The quartz textures are similar to those from other deformation zones where the deformation regime is

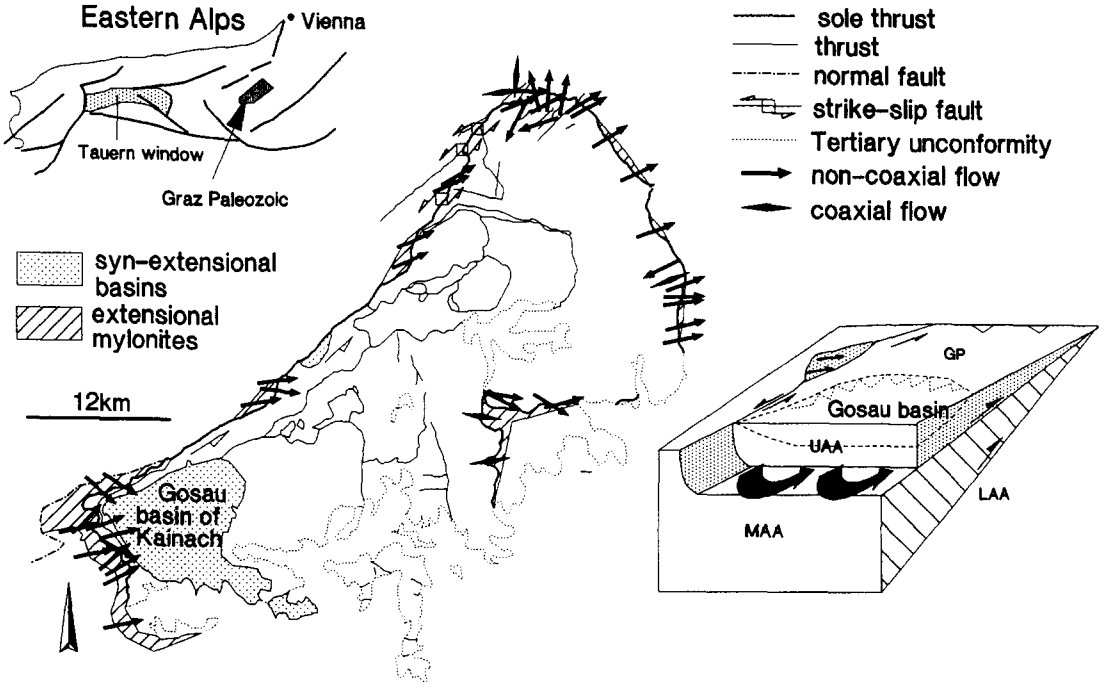

Fig. 2. Mylonites at the base of the Graz-Paleozoic thrust system, orientation of stretching lineations, and syn-extensional basin (Gosau basin of Kainach). Inserts locate the Graz-Paleozoic in the Eastern Alps and give a three-dimensional interpretation. UAA and MAA units wedge out toward the east.

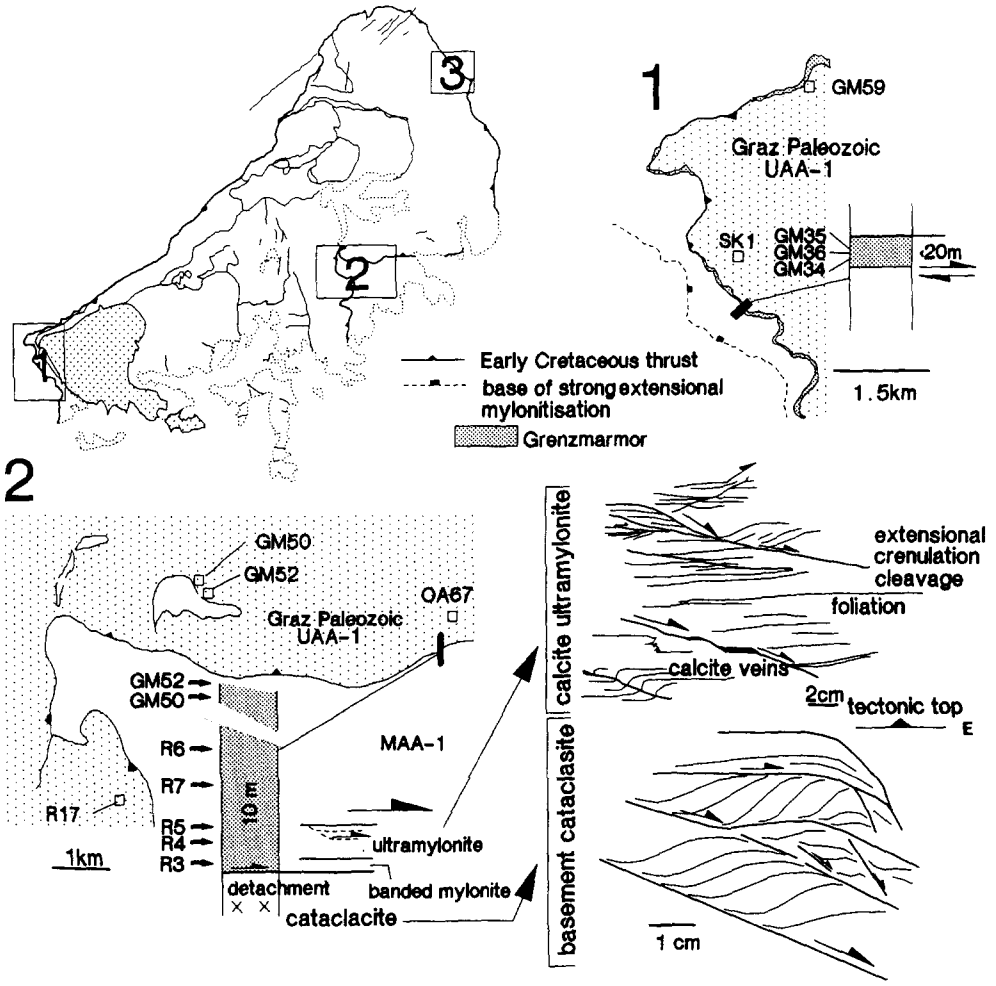

Fig. 3. Location of the studied profile sections (see also Fig. 4, top row) at the base of the Graz Paleozoic. 1: Western edge, map and sample localities. Insert gives profile across "Grenzmarmor" (GM). 2: Southeastern edge, map and sample localities; insert gives profile across "Grenzmarmor". Line drawings of structures in outcrops document heterogeneous flow in calcite ultramylonite above the detachment (spaced and domainal distribution) and in basement below the detachment.

established by independent criteria (e.g. Schmid & Casey 1986, Law *et al.* 1990). The texture asymmetry and the small-scale shear criteria imply a top-to-east sense of shear which is in accordance with regional tectonics.

Based on the mapping of the foliation and the microkinematic analysis, we propose a strain-path partitioning across the Graz-Paleozoic as displayed schematically in Fig. 1(b). A zone dominated by simple shear exists along the base and grades upwards into a zone in which pure shear dominates. Sigmoidally curving foliations, small-scale shear criteria, and asymmetric quartz textures are indicative of a simple shear zone. Horizontal foliation attitudes in the weakly deformed upper part of the Graz-Paleozoic and symmetric quartz textures signify the pure shear zone. Vertical strain-path partitioning in the Graz-Paleozoic resembles the vertical partitioning of theoretical spreading–gliding nappes. Ideally, we should study the horizontal variation of strain path to corroborate the spreading–gliding nappe interpretation of the Graz-Paleozoic. However, both root and toe of the nappe seem to have been cut off by erosion and such a study is not possible. We now use the qualitatively established strain-path partitioning to investigate how preferred orientation of calcite records this partitioning and assess how useful calcite textures are to determine the strain path at a particular locality.

Calcite textures. The macroscopic foliation as observed in the field is used as a reference plane and a stretching lineation as a reference direction to represent the textures of the calcite tectonites. This foliation is a complex structure reflecting both compositional banding and preferred orientation of minerals such as mica and opaques. It also reflects strain path by forming sigmoidal trajectories. Because of the high strains in the calcite tectonites (GM) the foliation is more or less parallel to the detachment surfaces (e.g. cross-sections, Fig. 4, top).

Table 1 summarizes the different measurements which describe the rock fabric. We recorded average grain ratio and grain size, and the number of mechanical twins per grain with a petrographic microscope. *c*-axis and twin preferred orientations on individual grains were measured with an U-stage. We derived incomplete pole figures of $(11\bar{2}0)$, $(10\bar{1}4)$ and $(01\bar{1}2)$ by X-ray

diffraction in reflection geometry; (0006) pole figures are difficult to measure directly. Instead, we calculated ODFs from the X-ray pole figures with the WIMV algorithm (Wenk *et al.* 1987) and recalculated [0001] and ($11\bar{2}0$) pole figures. These are displayed in Figs. 6 and 7. We do not represent full ODFs, because in our opinion it is unnecessary for typical calcite fabrics with a single *c*-axis maximum and *a*-axes oriented more or less randomly in a girdle. Particularly, ODF representations are not needed to assess texture asymmetry, which will be our main criterion to distinguish between pure and simple shear. Textures are displayed in fabric diagrams in lower-hemisphere, equal-area projections either as single point diagrams or contoured in multiples of a random distribution. Average grain shapes in two and three dimensions were determined by the R_f/ϕ (Lisle 1985) or Panozzo projection methods (Panozzo 1984). In addition, we determined the direction of maximum compressive stress (σ_1) from twin-*c*-axis sets by using three different methods. First, twin-*c*-axis pairs were plotted as fault–slickenside lineation pairs with the known slip sense from pole of lamellae to corresponding *c*-axis as displacement vector and the stress tensor orientation was calculated according to the direct inversion method of Angelier (1979). Secondly, the 'pressure'-axis, indicating the direction of σ_1 that would most effectively initiate twinning in each individual calcite grain, was derived by the method of Turner (1953). Thirdly, the method proposed by Dietrich & Song (1984) locates the direction of σ_1 in an area which contains a minimum number of host grain *c*-axis orientations and from which the lines which indicate translation directions caused by twinning diverge. We found good agreement between the three methods (Figs. 6 and 7, bottom rows). If twins form during the last stages of deformation, the σ_1 orientation should be at 45° to the shear plane in simple shear, and coincide with the foliation normal in pure shear. When both pure and simple shear contribute to the deformation, it is intermediate. However, if twins form throughout the defor-

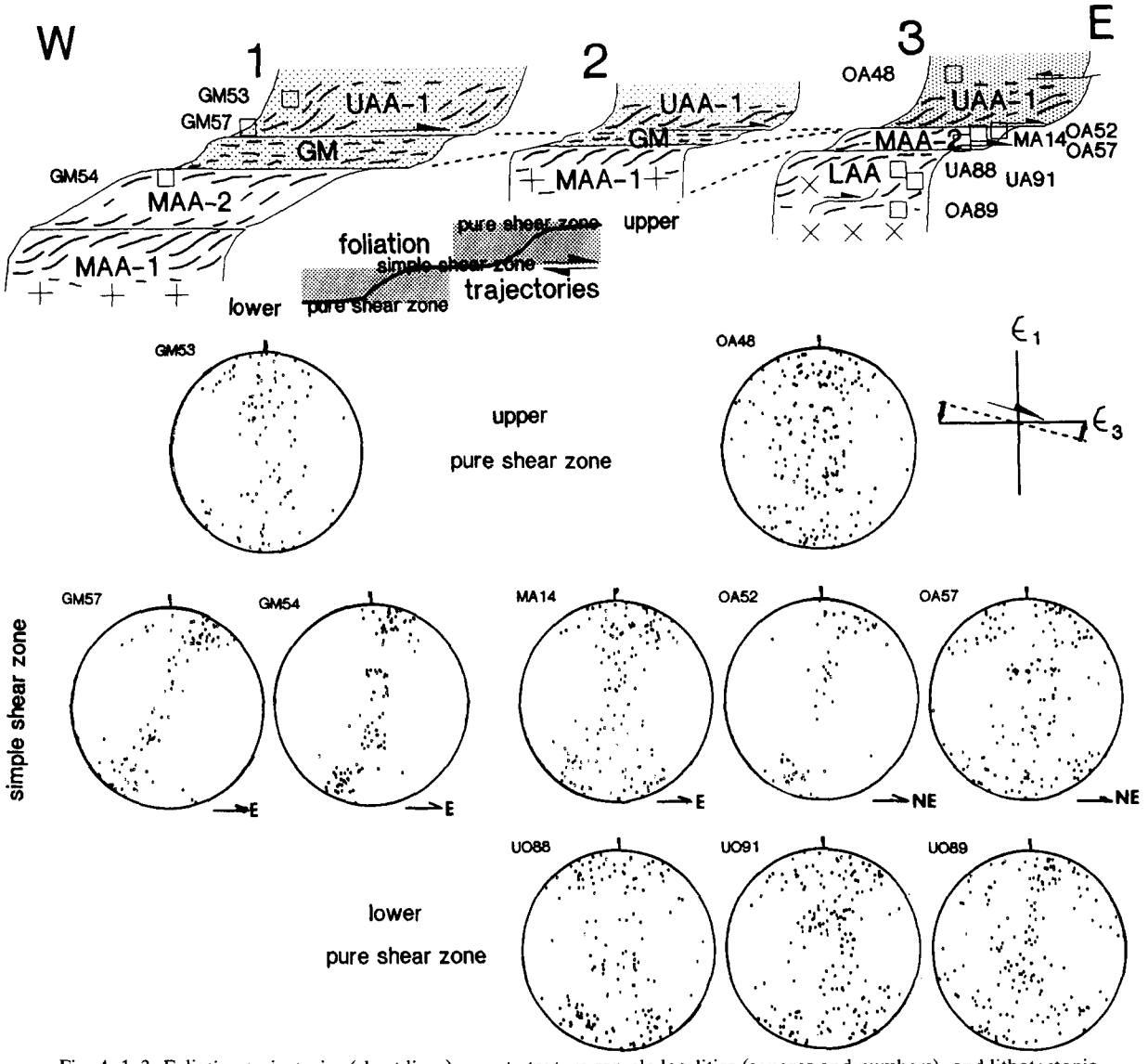

Fig. 4. 1–3, Foliation trajectories (short lines), quartz-texture sample localities (squares and numbers), and lithotectonic units [LAA, MAA: basement; UAA: Graz-Paleozoic (shaded); GM: calcite tectonites of the Grenzmarmor] in three schematic basal sections of the Graz-Paleozoic thrust sheet (not to scale; location see Fig. 3). Insert shows interpretation of the foliation trajectory pattern as zone of strain-path partitioning in pure and simple shear. The lower part displays quartz [0001] textures from the above units. Textures are displayed as equal-area (lower-hemisphere) projection fabric diagrams and are represented in respect to the finite strain axes (top right).

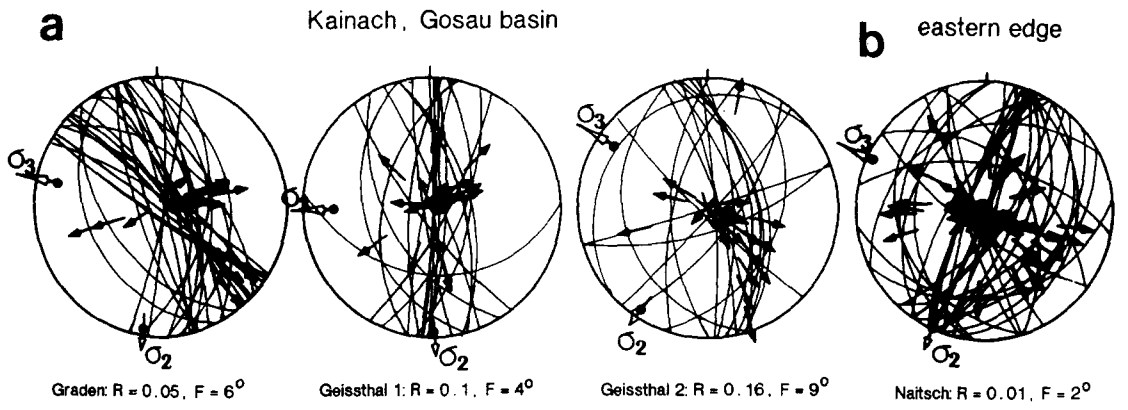

Fig. 5. Subhorizontal extension at high crustal level in the Graz-Paleozoic thrust sheet. (a) Hanging-wall sediments of the basin of Kainach at the western edge of the Graz-Paleozoic; (b) eastern margin of the Graz-Paleozoic. Stress analysis: raw data (faults and slickenside lineations) and principal stress orientations calculated by the direct inversion method of Angelier (1979); full circles: σ_1 ($\sigma_1 > \sigma_2 > \sigma_3$, σ_1 compressive; R: stress ellipsoid ratio, F: fluctuation as defined as average angle between computed shear stress orientations and observed slickenside lineations). Equal-area, lower-hemisphere projections.

mation history, old twins progressively rotate relative to the shear plane and σ_1 should be less than 45° to the slip plane also for simple shear histories.

At the western edge of the Graz-Paleozoic (Fig. 4, 1) the calcite-mylonites lie at the top of a highly deformed zone with eastward shearing (Fig. 3, 1). Calcite-textures were collected from the GM and the hanging marbles (UAA-1). GM34-36 cover the Grenzmarmor itself. The calcite grains in the GM are heavily twinned (≥38% of all grains) with a high percentage of grains containing two twin sets. Calcite grains are elongated (ratio in the XZ-section: 1.4–1.6:1), and the mean grain size is 0.2 mm (Table 1). In two specimens, grains define a plane of mean elongation which is inclined (10° and 15°, Table 1) to the mesoscopic foliation. The consistent sense of obliquity, used to infer shear sense (Simpson & Schmid 1983), indicates top-to-east shear.

[0001] and (11$\bar{2}$0) fabric diagrams and pole figures (Fig. 6) display a single maximum or girdle, respectively. In some samples the [0001] maximum is subnormal to the foliation, in others it is obliquely displaced against the geologically implied shear sense. We use an angle ω defined by Wenk *et al.* (1987) as the angle between the shear plane normal and either the [0001] maximum or the normal to the (11$\bar{2}$0) girdle to describe asymmetry (Fig. 6). Since we assume that in these strongly deformed samples the macroscopic shear plane is in close coincidence with the mesoscopic foliation this angle can

Table 1. Microstructural parameters

Specimen	Mean grain size	Mean grain shape	Texture asymmetry	Twin sets	σ_1 asymmetry
Western edge of Graz-Paleozoic					
GM34 X-ray			8°		
GM35 U-stage	0.15 mm		15°	62/35/3%	15°
GM36 U-stage	0.25 mm	R_f/ϕ: X/Z = 1.57:1			
		asymmetry: 10°	10°	12.5/38.5/46.5/2.5%	
SK1 U-stage			20°		
GM59 U-stage	0.2 mm	R_f/ϕ: $X:Y:Z$ = 1.4:1.2:1			
		k = 0.81			
		asymmetry: 15°	10°	32/44/19/5%	5°
Southeastern edge of Graz-Paleozoic					
R3 X-ray	strongly bimodal	R_f/ϕ: $X:Y:Z$ = 2.4:1.6:1	2°	65/35%	2°
	≤0.01 mm, 0.06 mm			coarse grains	
R4 X-ray			3°		
R5 X-ray			2°		
R7	strongly bimodal	R_f/ϕ: X/Z = 3/1	5°	81/19%	0°
U-stage	0.015 mm, 0.1 mm			coarse grains	
R6 X-ray	strongly bimodal	R_f/ϕ: $X:Y:Z$ = 4.2:2.5:1	8°	92/8%	
	≤0.01 mm, 0.05 mm	k = 0.45		coarse grains	
GM50 X-ray			10°		
GM52	bimodal	projection method	15°	72/25/3%	5°
U-stage	0.03 mm, 0.06 mm	X/Z = 1.53/1			
R17	slightly bimodal	R_f/ϕ: X/Z = 1.43/1	5°	84/15/1%	
U-stage	0.04 mm, 0.1 mm				
OA67	0.05 mm		20° (backflow)	60/38/2%	
U-stage	(heterogeneous)				
Morcles nappe					
Hv5 X-ray			20°		
Hv8 X-ray			20°		

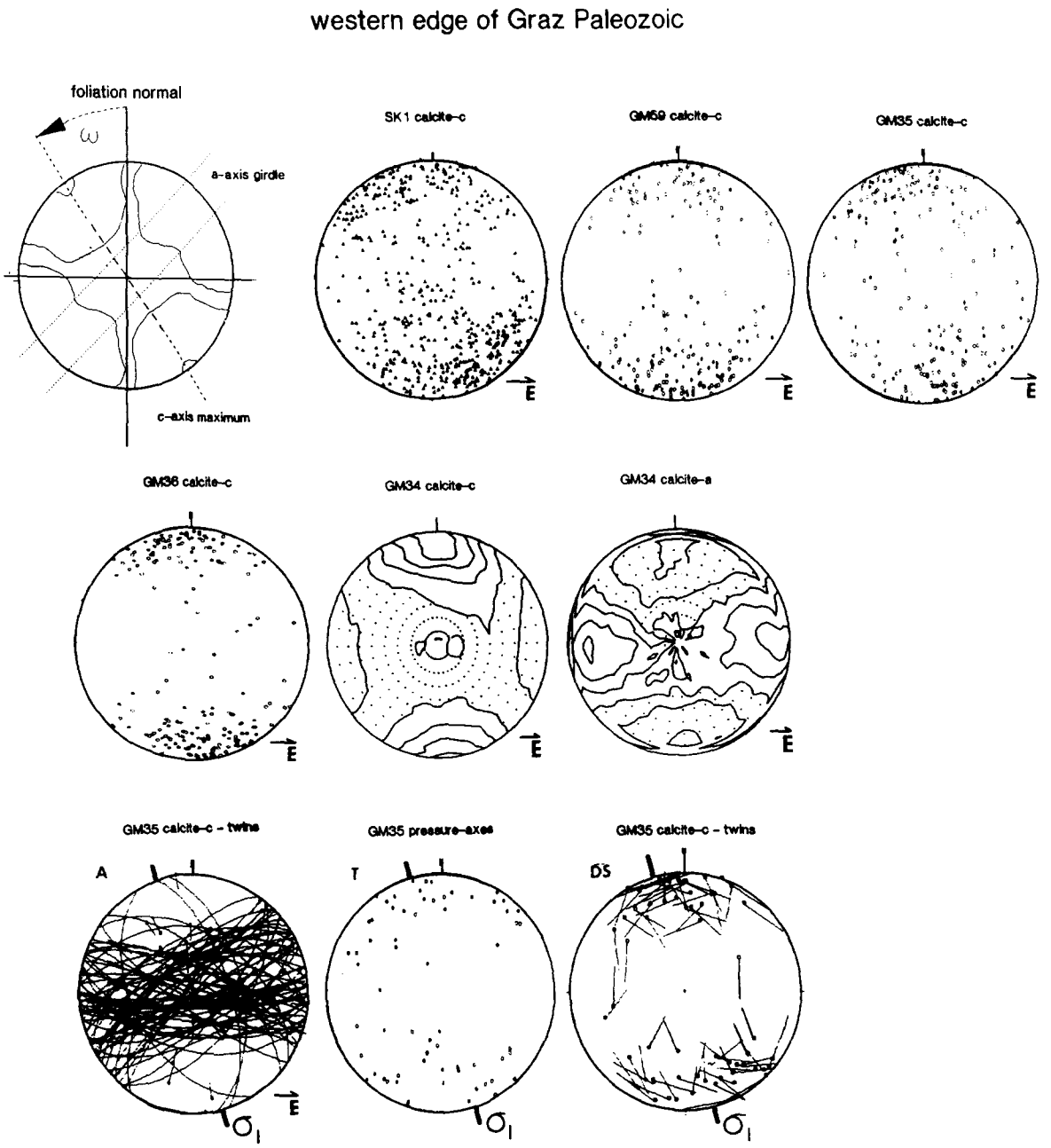

Fig. 6. Definition of fabric-asymmetry: ω, angle between the line connecting the [0001] maximum or the $(11\bar{2}0)$ girdle normal and the foliation normal. Calcite *c*- and *a*-axis pole figures, twin planes, and direction of maximum compressive stress (σ_1) from the western part of the Graz-Paleozoic. Lower-hemisphere, equal-area plots; axes plots give U-stage data, contoured plots are fabric diagrams recalculated from ODFs derived from X-ray pole figures with the WIMV agorithm. *c*-axis contour interval 0.5 mrd, *a*-axis contour interval 0.2 mrd, dotted below 1 mrd. Twins are plotted as fault–slickenside lineation pairs with known slip sense from pole of lamellae to corresponding *c*-axis as displacement vector; methods for maximum compressive stress (σ_1) determination are those of Angelier (1979) (A), Turner (1953) (T), and Dietrich & Song (1984) (DS) (circles give pole to twin, end of line indicate *c*-axis of the host).

be easily read off from the measured pole figures. In highly deformed samples with strong preferred orientation, the asymmetry ranges between 8° (GM34), 10° (GM36) and 15° (GM35). In two macroscopically less deformed samples within the Graz-Paleozoic, which show a similar microstructure as the GM samples but weaker preferred orientation (Table 1, Fig. 6), texture asymmetry is 10° (GM59) and 20° (SK1). Thus texture asymmetry is similar throughout the wide zone of deformation along the western edge of the Graz-Paleozoic. Directions of principal compressive stress (σ_1, Fig. 6, Table 1) do not correspond with the foliation normal of the samples and are consistently offset against the regional sense of shear. σ_1 directions implied from the twin orientations are similar or less asymmetric than the *c*-axis pole figures.

In the southeastern section (Fig. 4, 2) deformation is concentrated in a thin layer (a few meters) of mylonite and ultramylonite (GM, Fig. 3, 2) and is heterogeneous in the profile. Cataclasites dominate in the crystalline basement below the detachment fault; spaced heterogeneous deformation structures (normal faults and brittle–ductile shear zones, Fig. 3, 2) are common. Light–dark banded calcite ultramylonites (R3), ultramy-

lonites (R4, R5) with spaced, locally abundant, spectacular heterogeneous deformation structures (narrow brittle–ductile secondary shear bands; extensional crenulation cleavage of Platt & Vissers 1980; Fig. 3, 2), and massive, fine-grained mylonites (R6, R7, GM50, GM52), all without a prominent stretching lineation, overlie the detachment fault. Specimens R17 and OA67 are massive hanging-wall marbles (Fig. 3).

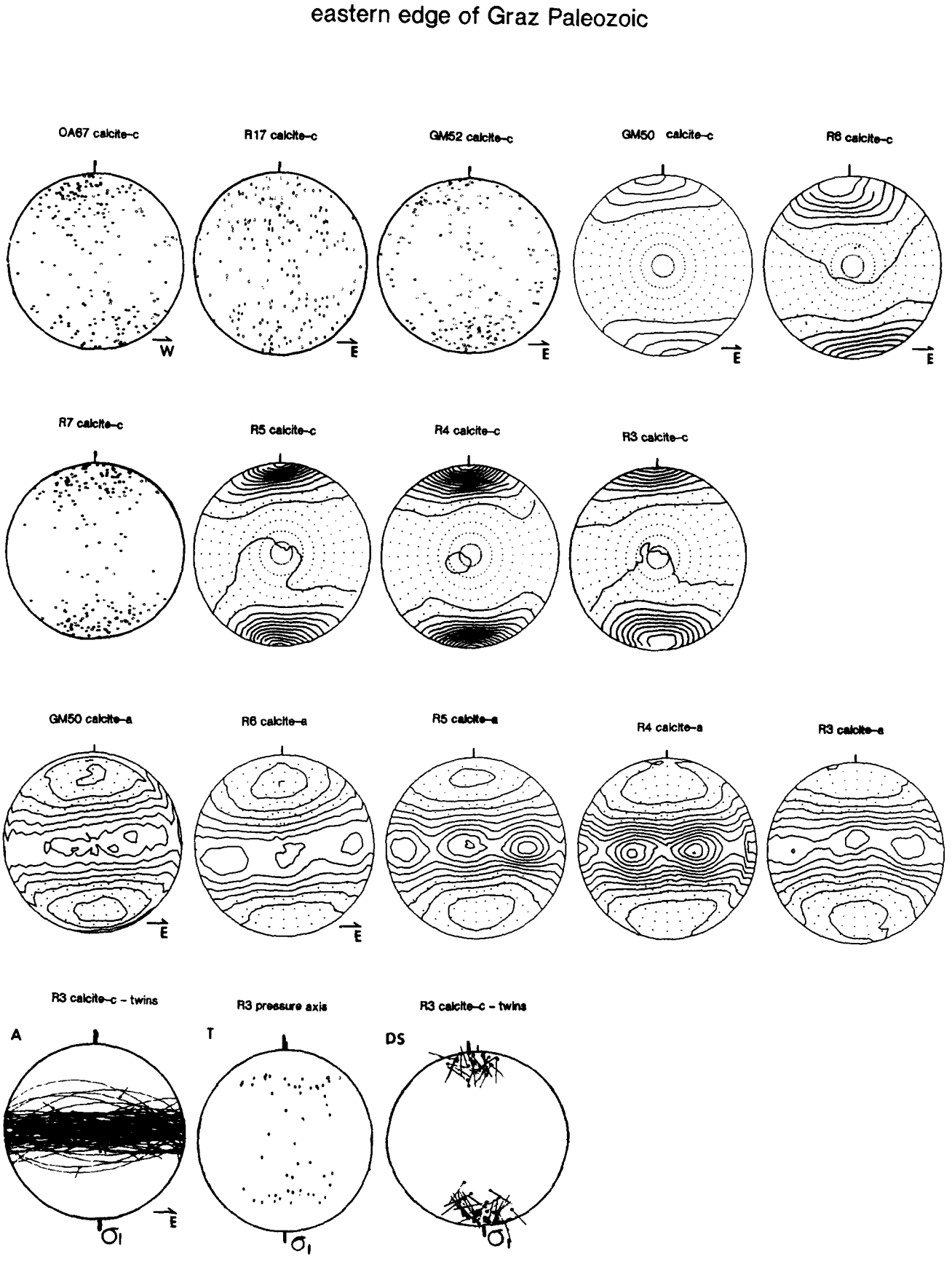

Fig. 7. Calcite-texture data from base of the southeastern section of the Graz-Paleozoic. For explanation see Fig. 6.

All calcite tectonites at this locality show a bimodal grain size distribution with equant fine grains and heavily twinned larger grains (Fig. 8a). The latter contain one well-ordered twin set (Fig. 7, Table 1). The mesoscopically high-strain appearance is reflected by the elongation of the relictic large grains (X/Z axial ratios: 2.5–4.2/1; Table 1). Their grain shape is slightly oblate (Table 1). Textures are strong and orthorhombic (R3–R5, Fig. 7 and Table 1). The massive, fine-grained mylonites above the ultramylonites display weak asymmetries (R6, R7, Table 1 and Fig. 7) and are transitional to the most pronounced asymmetries recorded in the calcite mylonites at the edge of the high-strain zone (GM50, GM52). The overlying marble has a weak texture and is nearly orthorhombic (Fig. 7). Specimen OA67 from within the zone of backflow shows asymmetry indicating top-to-west flow. Directions of maximum compressive stress (σ_1, Fig. 7 and Table 1) in the mylonites and ultramylonites correspond with the foliation normal.

Two observations surprise us: first, texture asymmetry and offset of the compressive stress axes is less pronounced or does not occur in the ultramylonites for which we assumed a strain path with a dominant simple shear component on the theoretical pattern of strain-path partitioning in the spreading–gliding model, the foliation and quartz texture mapping, and the distributed narrow sets of brittle–ductile shear bands. Secondly, although both the bimodal grain-size distribution and the equant fine-grained optically untwinned grain portion of the ultramylonites indicate a grain-boundary dominated flow mechanism, this is not supported by the presence of strong textures and the well-developed pervasive dislocation microstructure including microtwinning. Even in grains less than 0.5 μm in size, there are tangles of dislocations with high densities not just at grain boundaries (Figs. 8b & c). Microtwinning occurs in larger crystals, but is not common. Dislocation-creep mechanisms must have been dominant.

HELVETIC MORCLES NAPPE (SWISS ALPS)

As a comparative example for texture development in a nappe with a geologically well defined strain path, we now use the detailed deformation and texture data of the Morcles nappe in western Switzerland.

Structural setting

Various models have been proposed for the shape and internal deformation for the large-scale recumbant fold nappes of western Switzerland. These range from a model where a nappe thrusted over a ramp and was successively sheared (Ramsay *et al.* 1983), a thin-skinned model (Butler 1985), an extrusion–spreading model (Merle 1989) to a purely extrusional model (Dietrich & Casey 1989). The latter two are favored by the available strain and geometric data (Fig. 1c) (see reviews by Dietrich & Casey 1989, Ramsay 1989).

Strain increases from top to bottom and decreases from back to front. In a vertical section parallel to the transport direction, foliation trajectories are concave, steeply dipping toward the top and flat-lying toward the bottom. Sigmoidal trajectories occur toward the front of the nappes. This pattern is indicative of a strong simple shear component at the base of the nappes. Pure shear components are superposed at the rear and, probably, at the front of the nappes. At the rear they are related to subhorizontal orogenic compression and led to the extrusion between rigid basement slices (Dietrich & Casey 1989). At the front they are reflected by the downward concave foliation trajectories and may be related to a viscous spreading component (Merle 1989). Based on the foliation trajectory mapping (e.g. Dietrich & Casey 1989) and the microkinematic analysis (e.g. Schmid *et al.* 1981, Dietrich & Song 1984, Dietrich & Durney 1986), we propose a strain-path partitioning in the Morcles nappe which has a simple shear distributed throughout the nappe (see Dietrich & Casey 1989), pure shear superposed at the front and within the zone of extrusion, and a strong additional component of simple shear at the root where strain increases drastically from the weakly deformed basement below the nappe (Fig. 1d).

Calcite textures

We collected two samples of Jurassic limestone from the base of the Morcles nappe east of Lac Devant (Grand Chavalard, Fig. 1d) and determined textures by X-ray diffraction as described above (Fig. 9). Both show strong asymmetries (ω = 20°), but one sample has a much better developed texture than the other one. The asymmetry compares well with texture studies along the base of the western Helvetic nappes by Schmid *et al.* (1981), Dietrich & Song (1984) and Dietrich & Durney (1986). They observed texture asymmetries between 11° and 34° with two samples having asymmetries over 40°.

DISCUSSION

Texture orientation

In deformation studies and particularly for interpretations of preferred orientation patterns reference co-ordinates need to be established. Studies of texture simulations (e.g. Lister *et al.* 1978, Wenk *et al.* 1989, and references therein) use a co-ordinate frame based on shortening and elongation direction in pure shear (Fig. 10a), and on shear plane and shear direction in simple shear (Fig. 10b). For the latter, finite strain co-ordinates can easily be calculated given the shear strain. For an intermediate plane strain path, we consider only the special case in which the shear plane (simple shear) is perpendicular to the shortening direction (pure shear; corresponding to Fig. 10) and describe it with a plane strain displacement gradient tensor in analogy with Wenk *et al.* (1987, p. 740) as

$$\begin{pmatrix} D_{11} & D_{12} \\ 0 & -D_{11} \end{pmatrix}$$

which describes the incremental distortion of the polycrystal. There are of course other possibilities for plane strain paths intermediate between pure and simple shear which we have not described in our simulations. This reference frame for the displacement gradient tensor (xy, Fig. 10) has the advantage that it is physically fixed and does not rotate during deformation as is the case for the finite strain frame.

Samples collected in the field, are universally oriented with respect to the macroscopic foliation and lineation (as we did in this study). The reason for this choice is that shear planes are infrequently observed directly in rocks. For a dynamic intepretation of texture data the finite strain reference frame is not too useful, because it changes locally with the amount and degree of noncoaxial deformation. For our strongly deformed calcite tectonites, we assume that foliation and lineation are in close coincidence with the macroscopic shear plane and shear direction, respectively. Discrepancies are expected to be most serious if simple shear dominates and intensity of total deformation is low. At high total strain and with increasing pure shear the shear plane and an empirically defined foliation are most likely in close coincidence. We justify this assumption by the fact that due to the high strains in the calcite tectonites the foliation is more or less parallel to the detachment surfaces (e.g. cross-sections, Fig. 4, top), and pure shear is part of the strain path in all samples (see later).

Calcite texture development

The calcite textures described in this study are generally similar: c-axes are aligned subparallel to the foliation normal or are rotated away from this axis against the sense of shear. The best interpretation of textures relies on comparison of natural ones with those produced experimentally under similar conditions. This can be difficult because geological conditions can often not be reproduced. For example plane strain experiments are scarce (e.g. for pure shear Kern 1971, 1977, 1979, Wagner *et al.* 1982, Wenk *et al.* 1987, for simple shear Rutter & Rusbridge 1977, Friedman & Higgs 1981, Kern & Wenk 1983, Schmid *et al.* 1987). The pure shear experiments document a fabric transition. The textures produced at low temperature and with coarse-grained material correspond well with natural textures, those at high temperature and with fine-grained limestone are more complex (see review by Wenk 1985). In all low-temperature experiments deformation mechanisms were slip and mechanical twinning.

If deformation occurs by slip and twinning, texture evolution can be predicted with polycrystal plasticity theory. This is much more general and allows us to simulate deformation histories which are not accessible to direct experimentation. The Taylor (1938) theory was reasonably successful in reproducing experimental plane-strain textures (e.g. Wenk *et al.* 1986, 1987, Takeshita *et al.* 1987). Particularly the c-axis maximum texture is predicted when slip of $r^- = \{10\bar{1}4\}\langle 20\bar{2}1\rangle$ and mechanical twinning on $e^+ = \{1018\}\langle 40\bar{4}1\rangle$ are the dominant mechanisms.

We have recently applied modifications of the Taylor approach to quartz and observed considerable differences when rate sensitivity is accounted for and when local heterogeneous deformation is permitted (Wenk *et al.* 1989). Both rate sensitivity and heterogeneous deformation can be modelled with a self-consistent theory which satisfies both stress equilibrium and strain compatibility. We have explored the effects of viscoplasticity, relaxed constraints and self-consistent conditions for calcite and observed relatively minor differences compared to quartz (Tomé *et al.* in press). Texture simulations for 50% deformation in pure and simple shear in topologic domain E of Takeshita *et al.* (1987), which most closely matches natural conditions, are shown in Fig. 11 for the viscoplastic self-consistent model. Two models are illustrated. In one the critical resolved shear stress for e^+ twinning is relatively high, in the second one it is five times lower. Where twinning dominates, textures are sharper but the patterns are similar, also similar to rigid–plastic Taylor simulations (Wenk *et al.* 1986). In all cases, we observe in simple shear a c-axis maximum inclined about 36° to the shear plane normal against the sense of shear. The a-axis pole figures display a more or less continuous girdle perpendicular to the c-axis maximum. However there is a slight concentration of $(11\bar{2}0)$ poles in the ε_2 direction (and 60° from it) which agrees with all the natural $(11\bar{2}0)$ pole figures (Figs. 6 and 7) except R4. We suggest that deviations from plane strain or a more complicated strain path may be responsible for this discrepancy. In self-consistent simulations weak slip systems are favored compared to Taylor. Figure 12 shows slip system activities for the two models for which textures are illustrated in Fig. 11. r^- and e^+ are the main mechanisms which are active. Initially twinning dominates, particularly where twinning is favored (Fig. 12b), but its importance is reduced quickly with ongoing deformation. Twinned grains are rarely in a favorable orientation to twin again. After 50% deformation the same slip systems are active in both models and the similarity in texture is not surprising. In Taylor simulations also f^- needed to be activated to produce a homogeneous deformation.

In these diagrams (Fig. 12), we have also plotted the effective yield stress (in arbitrary units) as a function of texture evolution. In model (a) there is moderate softening, slightly more significant in pure shear. In model (b) the material hardens due to the reduced activity of easy twinning. The softening effect for pure shear which was documented in Taylor simulations (Wenk *et al.* 1987) is less pronounced for self consistent simulations, but at this point it is unclear which polycrystal plasticity model more adequately describes the deformation of limestone.

We again use the plasticity theory to approach the problem of strain-path partitioning between pure and simple shear and refer to Wenk *et al.* (1987) for details.

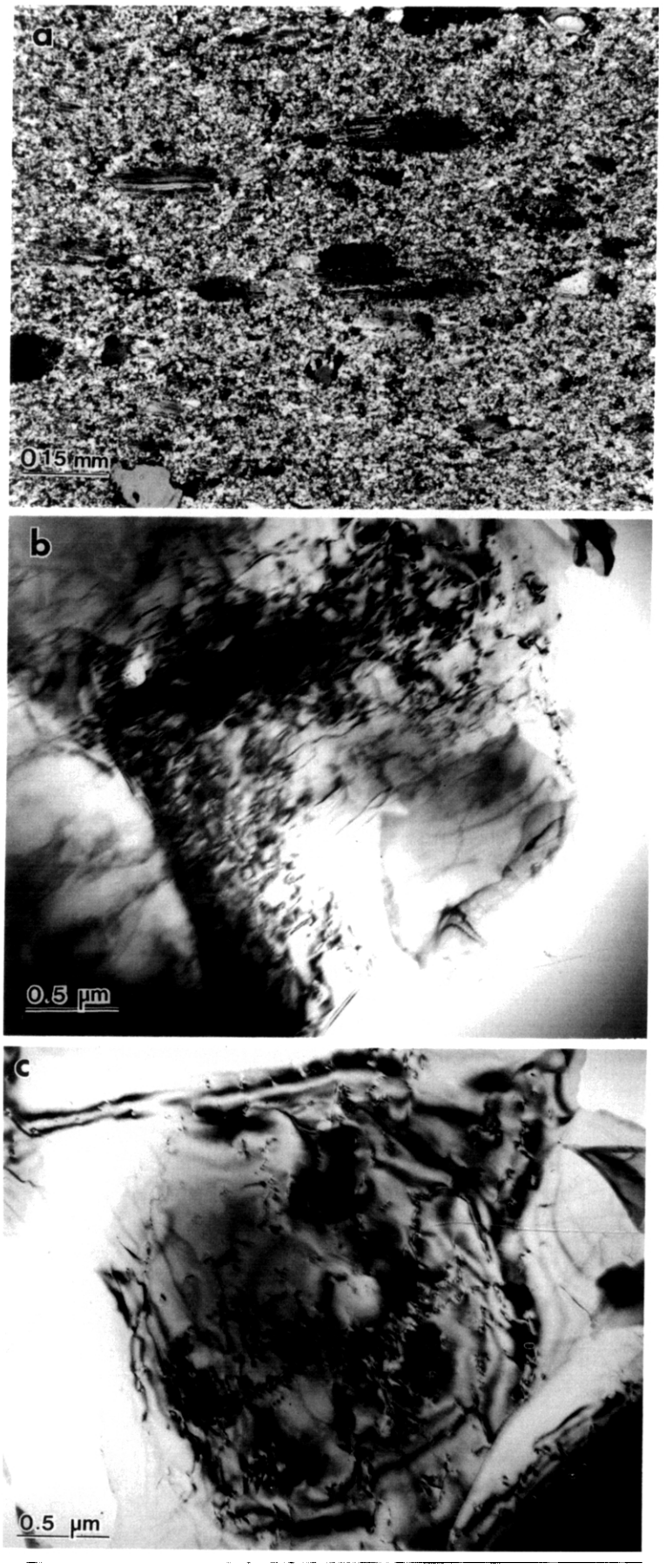

Fig. 8. (a) Thin-section photomicrograph of ultramylonite specimen R3. Note bimodal grain size and preferred orientation of *e*-twins in large grains. (b) TEM photomicrograph of specimen R3 with dislocation tangles in 2.5 μm grain. Note small, nearly dislocation-free grain in the lower right-hand corner indicating syntectonic recrystallization. (c) TEM photomicrograph of specimen R6 with dislocations partially arranged in subgrain boundaries. Dislocation densities are high in both ultramylonite specimens.

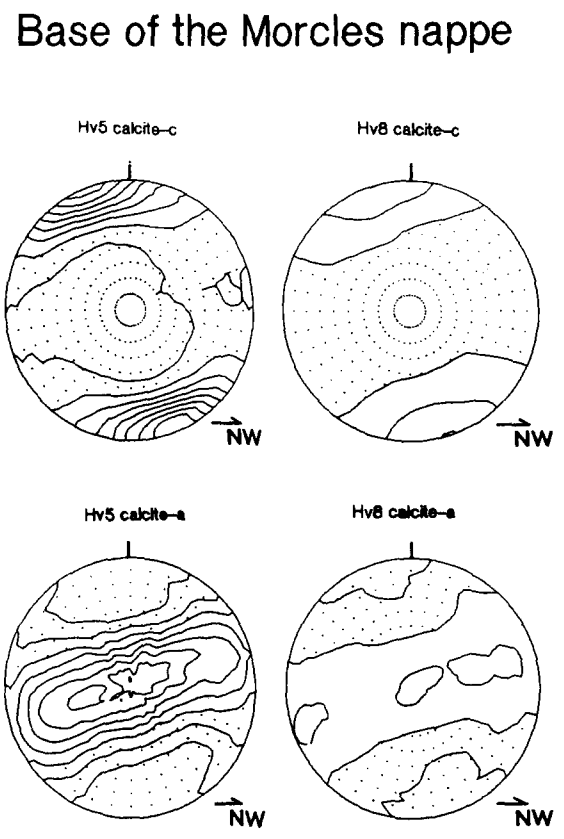

Fig. 9. Calcite-texture data from the Jurassic limestone at base of Morcles nappe east of Lac Devant (Grand Chavalard). For explanation see Fig. 6.

From simulations with the Taylor theory or the self-consistent model it is apparent that in simple shear strong textures develop with a [0001] maximum which is inclined about 36° to the shear plane normal (and does not change its position with increasing shear strain) whereas the pure shear textures are symmetric (Fig. 11). If the strain path is intermediate between pure and simple shear, the asymmetry ω of the maximum decreases with increasing fraction of pure shear. It varies almost linearly with the relative amount of simple and pure shear. Based on the Taylor simulations a determinative chart has been constructed which is shown in Fig. 13. Percentage of simple shear is defined in terms of displacement–gradient tensor components (see above) as in Wenk *et al.* (1987, table 3): $\% = 100 \cdot D_{12}/(2D_{11} + D_{12})$ for the geometry shown in Fig. 10.

Plotting of natural textures in this determination chart, represented in finite strain co-ordinates, poses the co-ordinate-system problem. Suppose a shear strain of 10, the asymmetry (Fig. 10c) would be 36° in a simulated

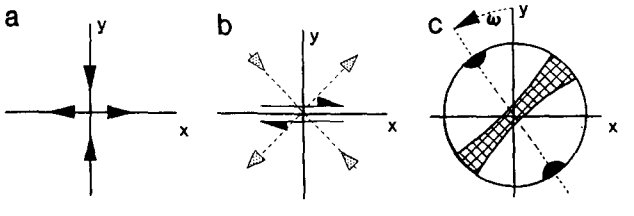

Fig. 10. Definition of the co-ordinate system used in texture simulations: (a) pure shear; (b) simple shear; (c) asymmetry angle ω in pole figures.

texture using the kinematic frame. In a natural texture, using the finite strain frame, the asymmetry would be about 42° (in simple shear, the angle θ between the principal axis of finite strain and the shear plane are related by $\tan 2\theta = 2/\gamma$). As mentioned above, discrepancies are expected to be most serious for simple shear and low intensity of total deformation. They are small at high total strain and with increasing pure shear. In our samples we believe that discrepancies are small for the following reasons. (1) Strain, as assessed from the macroscopic defomation fabric, seems to be high in all calcite mylonites (e.g. at shear strains ≥ 10, errors would be $\leq 5.56°$). This assumption is compatible with the observation that the mylonitic foliation in the calcite tectonites is subparallel to the bounding detachments. (2) Pure shear is part of the strain path in all samples. This is evident from the distribution of samples along the curve in Fig. 13 and follows from the strain path of theoretical spreading–gliding nappes. Also, classification of samples into distinct groups with characteristic strain paths remains unaffected by small shifts along the curve in Fig. 13.

Calcite textures from Alpine nappes which we expected to have deformed in a path intermediate between pure and simple shear do show a large spread in texture asymmetry. The asymmetry correlates qualitatively well with the amount of simple shear expected for the base of the Graz-Paleozoic except for the zone in the immediate vicinity of the basal detachment fault. It correlates also qualitatively well with the zone of combined simple and pure shear in the extrusion zone at the root of the Morcles nappe.

All calcite textures discussed in this study plot on Fig. 13 except for two from the Helvetic nappes (Dietrich & Song 1984) which have a higher asymmetry than the texture simulations allow. This could either be due to (1) uncertainties in identifying the macroscopic strain reference-frame, (2) a shortening subparallel to the shear zone caused by superposition of deformation events (Dietrich & Durney 1986) or (3) due to the selection of the finite strain co-ordinate system and low strain intensity. Based on Fig. 13, we estimated that in the Graz-Paleozoic calcite tectonites simple shear contributes 0–60% to the deformation. Whereas the variation in the amount of simple shear is continuous across the western edge of the Graz-Paleozoic, deformation occurs almost entirely by pure shear in the zone of ultramylonites at the southeastern edge of the Graz-Paleozoic. In our two samples from the Morcles nappe simple shear contributed 60% and in the samples from the Helvetic nappes in western Switzerland taken from the literature it contributed between 35 and 100%.

Strain-path partitioning

Most textures of calcite tectonites reported in this study (western edge of Graz-Paleozoic, Morcles nappe, Fig. 13), and other studies from the Central Alps (Helvetic nappes, Fig. 13), indicate a significant component of simple shear (>30%) in the overall deformation.

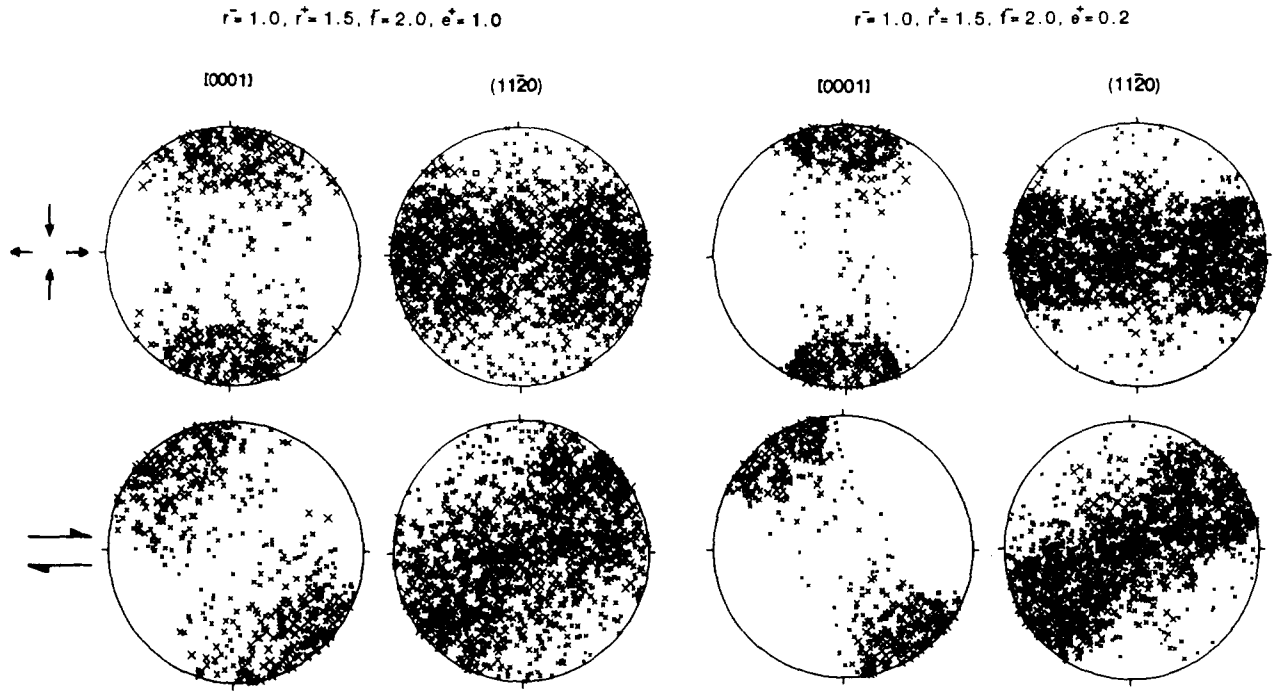

Fig. 11. Viscoplastic self-consistent texture simulations of calcite deformed in pure shear and simple shear. Top: critical resolved shear-stress ratios for both models. 500 grains, 50% strain, equal-area projection, [0001] and (11$\bar{2}$0) fabric diagrams. The larger the symbol size the stronger the deformation of the individual grains.

However, a striking aspect is the concentration of pure shear deformation in a narrow zone at the base of the Graz-Paleozoic.

Partitioning of strain-path in thrust sheets has already been described in several studies (e.g. Sanderson 1982, Law *et al.* 1984, Platt & Behrmann 1986, and references therein). In terms of vertical partitioning, however, the opposite was recorded as in our study. For example, Law *et al.* (1984) and Platt & Behrmann (1986) found a marked gradient of simple shear, which *increased* toward the sole thrust. Lister & Williams (1983), on largely theoretical grounds, concluded that in the presence of (planar) material anisotropies (e.g. foliation) advantage is taken of these planes of weakness and a non-coaxial strain path, e.g. progressive simple shear, is favored on the scale of the movement zone. However, the presence of unconstrained (or weakly constrained) boundaries (which represent surfaces of no shear stress) allow the intervening material to rotate freely. Thus,

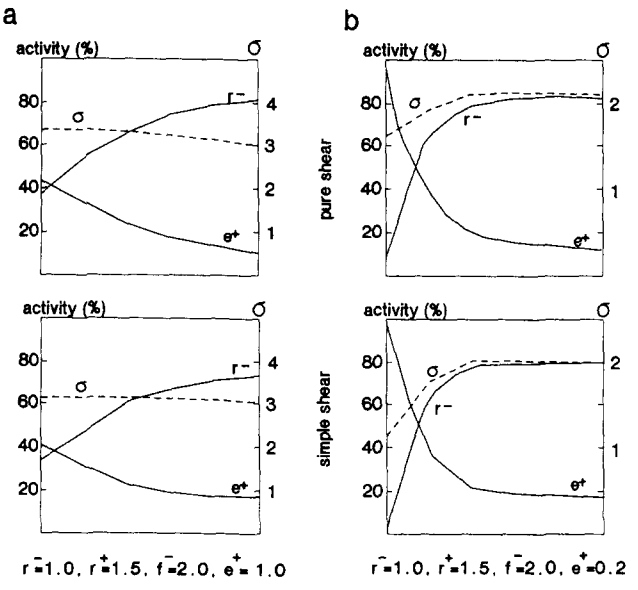

Fig. 12. Slip-system activities for e^+ and r^- (in %) for model calculations shown in Fig. 11. In (a) twinning is five times harder than in (b). Also shown are effective yield stress curves (σ) illustrating hardening or softening with texture development; compare to fig. 15 of Wenk *et al.* (1987) for Taylor simulations.

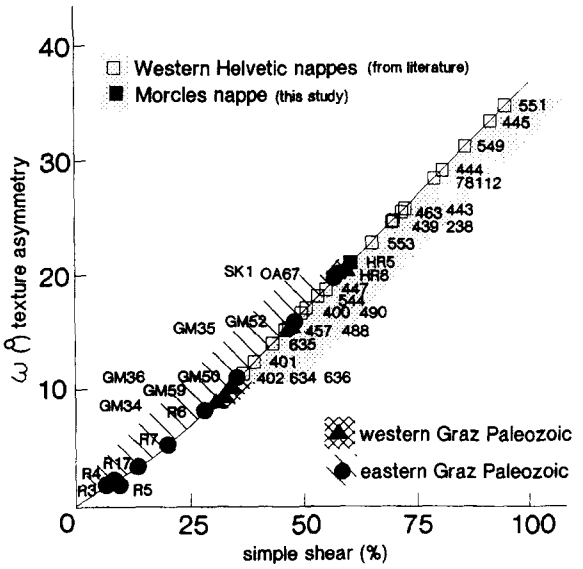

Fig. 13. Texture asymmetry (definition Fig. 10c) vs percentage of simple shear in bulk flow samples from the Graz-Paleozoic and the western Helvetic nappes (data from this study and Schmid *et al.* 1981, Dietrich & Song 1984, Dietrich & Durney 1986). Line gives correlation function determined from texture simulations using the Taylor theory (from Wenk *et al.* 1987). Percentage of simple shear is defined in terms of displacement–gradient tensor components: $\% = 100 \cdot D_{12}/(2D_{11} + D_{12})$.

when the intervening material is caused to deform, it undergoes a combination of coaxial extension and rotation (Fig. 14a). Lister & Williams (1979) and Platt & Behrmann (1986) suggested that, although the bulk deformation may approximate to simple shear, smaller volumes of the movement zone may follow coaxial strain paths. Sliding goes on along discontinuities, but the rock between the discontinuities suffers a coaxial strain path with extension parallel to the foliation planes (plastic card deck model of Platt & Behrmann 1986). The instantaneous stretching axes rotate as the foliation rotates. Sliding, however, becomes less important as deformation goes on. A first explanation for the concentration of pure shear deformation, thus, may be that the base of the Graz-Paleozoic was subjected to a coaxial strain path due to the presence of the basal detachment while the bulk deformation was progressive simple shear (Fig. 14a).

We favor as an explanation the possibility of 'work softening' which is suggested by Taylor calculations (fig. 15 of Wenk *et al.* 1987). They indicate that (1) calcite tectonites become weaker with increasing strain and (2) pure shear deformation is energetically favorable over simple shear. Such 'texture softening' may induce instabilities to local ultramylonite zones. This would corroborate recent observations of calcite textures in strongly deformed tectonites in several metamorphic core complexes in the western United States (Erskine & Wenk 1985, Erskine *et al.* in press) which also revealed highly symmetric fabrics.

In both models, the pure shear zone parallel to the base of the Graz-Paleozoic is limited from spreading laterally over a large distance due to compatibility problems in heterogeneous pure shear (e.g. Ramsay & Huber 1987, p. 611). A heterogeneous pure shear component with axes parallel to the deformation-zone walls cannot exist by itself. The high-strain pure-shear flow parallel to the detachment surface in the Graz-Paleozoic produces an overall displacement scheme which is accommodated by inducing both discontinuities and shear strain components adjacent to the coaxially deforming element.

Figure 14(b) sketches what we believe is the most probable accommodation model for the observed deformation and flow patterns at the base of the Graz-Paleozoic. Along the western edge, heterogeneous simple shear and homogeneous pure shear coexist. No compatibility problems arise. Along the eastern edge progressive deformation was concentrated in a mechanically weak layer deforming by pure shear. Strain incompatibilities were accommodated by faulting reflected in the basal detachment or by deformation along localized zones of heterogeneous simple shear. An expression of these zones are the dispersed heterogeneous flow structures (extensional crenulation cleavage) and the asymmetric textures indicating increased simple shear adjacent to the pure shear zone.

Abrupt changes in the vertical velocity profile across the basal zone may have caused localized backflow in shear and fault zones in the hanging wall of the main deformation zone. We consider the main body of the Graz-Paleozoic and the basement units below the zone of eastward flow as relatively rigid blocks, and propose that the backflow structures are caused by the complex flow pattern around the highly viscous calcite tectonites. This velocity profile may contain several lines of no shear strain with flow reversing across them. The schematic velocity profile indicated in Fig. 14(c) for the eastern margin of the Graz-Paleozoic may represent deviatoric components of the larger scale subhorizontal top-to-east velocity profile (see Schmid *et al.* in press for a large-scale natural example).

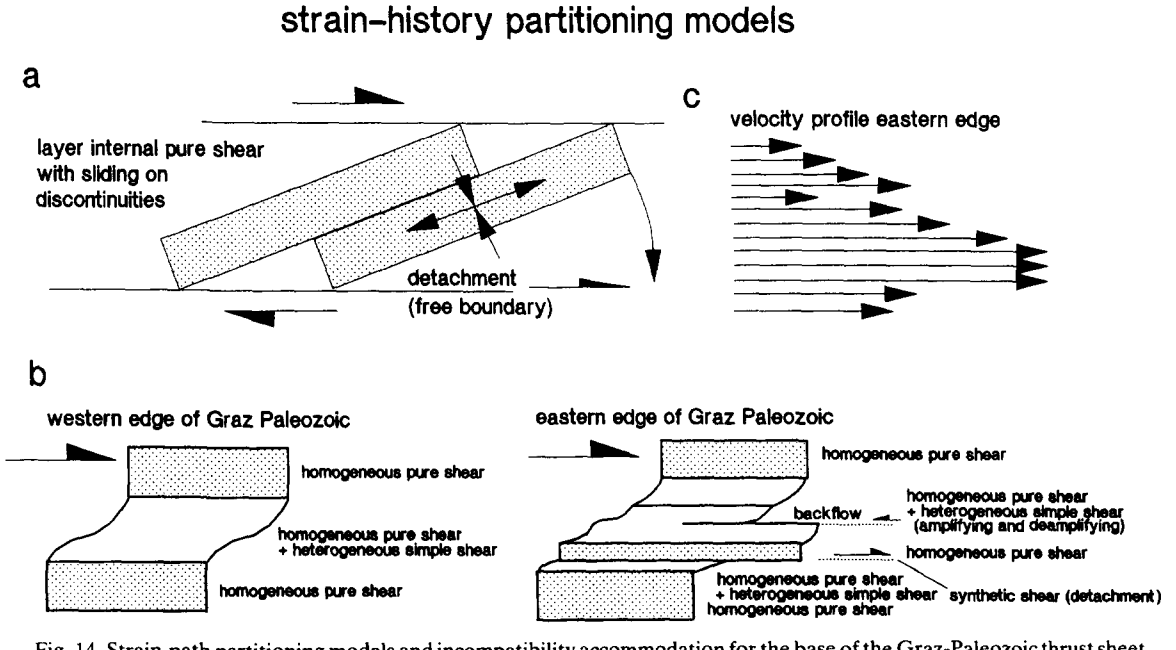

Fig. 14. Strain-path partitioning models and incompatibility accommodation for the base of the Graz-Paleozoic thrust sheet. (a) Small volumes of the movement zone follow coaxial strain-paths due to sliding along discontinuities. (b) Partitioning due to 'texture softening' in high-strain layers. (c) Velocity profile for the eastern section of the Graz-Paleozoic. See text for discussion.

Acknowledgements—L. Ratschbacher acknowledges the invitation to teach at UC Berkeley which provided time to complete this work. We were funded by grants Ra442/2-2 and Fr610/7-2 (L. Ratschbacher), from DFG and EAR-8709378 (H.-R. Wenk) from NSF. Jürgen Elias, Uwe Herrmann, and Blanka Sperner contributed with U-stage work. Florian Heidelberg assisted with X-ray measurements. Josef Nievoll provided part of the fault data displayed in Fig. 5. Reviews by R. Kligfield, J. P. Platt (as associate editor) and a third referee helped clarify concepts presented in this paper.

REFERENCES

Angelier, J. 1979. Determination of the mean principal directions of stresses for a given fault population. *Tectonophysics* **56**, T17–T26.

Butler, R. W. H. 1985. The restoration of thrust systems and displacement continuity around the Mont Blanc Massif, NW external Alpine thrust belt. *J. Struct. Geol.* **7**, 569–582.

Chapple, W. M. 1978. Mechanics of thin-skinned fold-and-thrust belts. *Bull. geol. Soc. Am.* **89**, 1189–1198.

Dietrich, D. & Casey, M. 1989. A new tectonic model for the Helvetic nappes. In: *Alpine Tectonics* (edited by Coward, M. P., Dietrich, D. & Park, R. G.). *Spec. Publs geol. Soc. Lond.* **45**, 47–64.

Dietrich, D. & Durney, D. W. 1986. Change of direction of overthrust shear in the Helvetic nappes of western Switzerland. *J. Struct. Geol.* **8**, 389–398.

Dietrich, D. & Song, H. 1984. Calcite fabrics in a natural shear environment, the Helvetic nappes of western Switzerland. *J. Struct. Geol.* **6**, 19–32.

Elliott, D. 1976. The motion of thrust sheets. *J. geophys. Res.* **81**, 949–963.

Erskine, B. G. & Wenk, H.-R. 1985. Evidence for Late Cretaceous crustal thinning in the Santa Rosa mylonite zone, southern California. *Geology* **13**, 274–277.

Erskine, B. G., Wenk, H.-R. & Heidelbach, F. In press. Texture development in calcite mylonites in the Western United States. *Bull. geol. Soc. Am.*

Friedman, M. & Higgs, N. C. 1981. Calcite fabrics in experimental shear zones. *Am. Geophys. Un. Geophys. Monogr.* **24**, 11–27.

Fritz, H. 1988. Kinematics and geochronology of early Cretaceous thrusting in the northwestern Paleozoic of Graz (Eastern Alps). *Geodin. Acta* **2**, 53–62.

Hobbs, B. E., Means, W. D. & Williams, P. F. 1976. *An Outline of Structural Geology*. Wiley, New York.

Kehle, R. O. 1970. Analysis of gravity sliding and orogenic translation. *Bull. geol. Soc. Am.* **81**, 1641–1664.

Kern, H. 1971. Dreiaxiale Verformung an Solnhofen Kalkstein im Temperaturbereich von 20°C–650°C, röntgenographische Gefügeuntersuchungen mit dem Texturgoniometer. *Contr. Miner. Petrol.* **31**, 39–66.

Kern, H. 1977. Preferred orientation of experimentally deformed marble, quartzite and rock salt at different temperatures and states of stress. *Tectonophysics* **38**, 103–120.

Kern, H. 1979. Texture development in calcite and quartz rocks deformed at uniaxial and real triaxial states of strain. *Bull. Minéral.* **102**, 290–300.

Kern, H. & Wenk, H.-R. 1983. Calcite texture development in experimentally induced ductile shear zones. *Contr. Miner. Petrol.* **83**, 231–236.

Law, R. D., Knipe, R. J. & Dayan, H. 1984. Strain path partitioning within thrust sheets: microstructural and petrofabric evidence from the Moine Thrust zone at Loch Eriboll, northwest Scotland. *J. Struct. Geol.* **6**, 477–497.

Law, R. D., Schmid, S. M. & Wheeler, J. 1990. Simple shear deformation and quartz crystallographic fabrics: a possible natural example from the Torridon area of NW Scotland. *J. Struct. Geol.* **12**, 29–45.

Lisle, R. J. 1985. *Geological Strain Analysis. A Manual for the R_f/ϕ Method*. Pergamon Press, Oxford.

Lister, G. S., Paterson, M. S. & Hobbs, B. E. 1978. The simulation of fabric development in plastic deformation and its application to quartzite: The model. *Tectonophysics* **45**, 107–158.

Lister, G. S. & Williams, P. F. 1983. The partitioning of deformation in flowing rock masses. *Tectonophysics* **92**, 1–33.

Merle, O. 1986. Patterns of stretch trajectories and strain rates within spreading-gliding nappes. *Tectonophysics* **124**, 211–222.

Merle, O. 1989. Strain models within spreading nappes. *Tectonophysics* **165**, 57–71.

Panozzo, R. 1984. Two-dimensional strain from the orientation of lines in a plane. *J. Struct. Geol.* **6**, 215–221.

Platt, J. P. 1986. Dynamics of orogenic wedges and the uplift of high-pressure metamorphic rocks. *Bull. geol. Soc. Am.* **97**, 1037–1053.

Platt, J. P. & Behrmann, J. H. 1986. Structures and fabrics in a crustal-scale shear zone, Betic Cordillera, SE Spain. *J. Struct. Geol.* **8**, 15–33.

Platt, J. P. & Vissers, R. L. M. 1980. Extensional structures in anisotropic rocks. *J. Struct. Geol.* **2**, 397–410.

Ramsay, J. G. 1989. Fold and fault geometry in the western Helvetic nappes of Switzerland and France and its implication for the evolution of the arc of the western Alps. In: *Alpine Tectonics* (edited by Coward, M. P., Dietrich, D. & Park, R. G.). *Spec. Publs geol. Soc. Lond.* **45**, 33–45.

Ramsay, J. G., Casey, M. & Kligfield, R. 1983. Role of shear in development of the Helvetic fold–thrust belt of Switzerland. *Geology* **11**, 439–442.

Ramsay, J. G. & Graham, R. H. 1970. Strain variation in shear belts. *Can. J. Earth Sci.* **7**, 786–813.

Ramsay, J. G. & Huber, M. I. 1987. *The Techniques of Modern Structural Geology, Volume* 2: *Folds and Fractures*. Academic Press, London.

Ratschbacher, L., Frisch, W., Neubauer, F., Schmid, S. M. & Neugebauer, J. 1989. Extension in compressional orogenic belts: the eastern Alps. *Geology* **17**, 404–407.

Ratschbacher, L. & Neubauer, F. 1989. West-directed décollement of Austro-Alpine cover nappes in the Eastern Alps: Geometrical and rheological considerations. In: *Alpine Tectonics* (edited by Coward, M. P., Dietrich, D. & Park, R. G.). *Spec. Publs geol. Soc. Lond.* **45**, 243–262.

Rutter, E. H. & Rusbridge, M. 1977. The effects of non-coaxial strain paths on crystallographic preferred orientation development in the experimental deformation of a marble. *Tectonophysics* **39**, 73–86.

Sanderson, D. J. 1982. Models of strain variation in nappes and thrust sheets: a review. *Tectonophysics* **88**, 201–233.

Schmid, S. M. & Casey, M. 1986. Complete fabric analysis of some commonly observed quartz *c*-axis patterns. *Am. Geophys. Un. Geophys. Monogr.* **36**, 263–286.

Schmid, S. M., Casey, M. & Starkey, J. 1981. The microfabric of calcite tectonites from the Helvetic Nappes (Swiss Alps). In: *Thrust and Nappe Tectonics* (edited by McClay, K. R. & Price, N. J.). *Spec. Publs geol. Soc. Lond.* **9**, 151–158.

Schmid, S. M., Panozzo, R. & Bauer, S. 1987. Simple shear experiments on calcite rocks: rheology and microfabric. *J. Struct. Geol.* **9**, 747–778.

Schmid, S. M., Rück, P. H. & Schreurs, G. In press. The significance of the Schams nappes for the reconstruction of the paleotectonic and orogenic evolution of the Penninic zone along the NFP 20 East traverse (Grisons, eastern Switzerland).

Simpson, C. & Schmid, S. M. 1983. An evaluation of criteria to deduce the sense of movement in sheared rocks. *Bull. geol. Soc. Am.* **94**, 1281–1288.

Takeshita, T., Tomé, C., Wenk, H.-R. & Kocks, U. F. 1987. Single-crystal yield surface for trigonal lattices: Application to texture transitions in calcite polycrystals. *J. geophys. Res.* **92**, 12917–12930.

Taylor, G. I. 1938. Plastic strain in metals. *J. Inst. Metals* **62**, 301–324.

Tomé, C. N., Wenk, H.-R., Canova, G. R. & Kocks, U. F. In press. Simulations of texture development in calcite: comparison of polycrystal plasticity theories. *J. geophys. Res.*

Turner, F. J. 1953. Nature and dynamic interpretation of deformation lamellae in calcite of three marbles. *Am. J. Sci.* **251**, 276–296.

Wagner, F., Wenk, H.-R., Kern, H., Van Houtte, P. & Esling, C. 1982. Development of preferred orientation in plane strain deformed limestone: experiment and theory. *Contr. Miner. Petrol.* **80**, 132–139.

Wenk, H.-R. 1985. Carbonates. In: *Preferred Orientation in Deformed Metals and Rocks. An Introduction to Modern Texture Analysis* (edited by Wenk, H.-R.). Academic Press, Orlando, Florida, 361–384.

Wenk, H. R., Canova, G., Molinari, A. & Kocks, U. F. 1989. Viscoplastic modeling of texture development in quartzite. *J. geophys. Res.* **94**, 17,895–17,906.

Wenk, H.-R., Kern, H., Van Houtte, P. & Wagner, F. 1986. Heterogeneous strain in axial deformation of limestone, textural evidence. *Am. Geophys. Un. Geophys. Monogr.* **36**, 287–295.

Wenk, H.-R., Takeshita, T., Bechler, E., Erskine, B. G. & Matthies, S. 1987. Pure shear and simple shear calcite textures. Comparison of experimental, theoretical and natural data. *J. Struct. Geol.* **9**, 731–745.